

IncSAR: A Dual Fusion Incremental Learning Framework for SAR Target Recognition

George Karantaidis

Athanasios Patsios

Yiannis Kompatsiaris

Symeon Papadopoulos

Information Technologies Institute, Centre for Research & Technology Hellas, Thessaloniki, Greece

{karantai, apatsios, ikom, papadop}@iti.gr

Abstract

Deep learning techniques have been successfully applied in Synthetic Aperture Radar (SAR) target recognition in static scenarios relying on predefined datasets. However, in real-world scenarios, models must incrementally learn new information without forgetting previously learned knowledge. Models' tendency to forget old knowledge when learning new tasks, known as catastrophic forgetting, remains an open challenge. In this paper, an incremental learning framework, called IncSAR, is proposed to mitigate catastrophic forgetting in SAR target recognition. IncSAR comprises a Vision Transformer (ViT) and a custom-designed Convolutional Neural Network (CNN) in individual branches combined through a late-fusion strategy. A denoising module, utilizing the properties of Robust Principal Component Analysis (RPCA), is introduced to alleviate the speckle noise present in SAR images. Moreover, a random projection layer is employed to enhance the linear separability of features, and a Linear Discriminant Analysis (LDA) approach is proposed to decorrelate the extracted class prototypes. Experimental results on the MSTAR and OpenSAR-SHIP benchmark datasets demonstrate that IncSAR outperforms state-of-the-art approaches, leading to an improvement from 98.05% to 99.63% in average accuracy and from 3.05% to 0.33% in performance dropping rate.

1 Introduction

Synthetic aperture radar (SAR) is an active remote sensing technology that obtains high-resolution images with minimal dependence on light, weather, and other environmental conditions. SAR automatic target recognition (SAR-ATR) through deep learning finds applications in a wide range of fields, such as target acquisition, disaster management, and maritime vigilance [1]. The interpretation of SAR images is considered to be a challenging task due to the presence of speckle noise. In contrast to optical images, SAR images tend to exhibit smaller inter-class and larger intra-class distances,

rendering their classification a hard challenge [2].

In practical settings, applications often deal with streaming data with incoming new classes that cannot be stored and recalled due to bounded storage. An additional challenge present in practical scenarios concerns data distribution shifts over time. Class incremental learning (CIL) aims to build models that continually adapt to new sets of classes while performing well among all seen classes. Catastrophic forgetting [3], a crucial issue present in incremental learning, refers to the phenomenon where a model's performance on previously learned tasks deteriorates as it acquires new knowledge. A relevant challenge in CIL involves the stability-plasticity trade-off [4], which refers to the balance between a model's ability to preserve old knowledge and its ability to adapt to new classes. Despite recent advancements in CIL methods, their performance remains significantly lower compared to conventional machine learning scenarios, especially in the face of an increasing number of incremental tasks.

One of the most popular CIL techniques includes regularization-based methods [5, 6], which use regularization terms and typically involve storing a frozen copy of the old model, imposing constraints on important weights, or implementing knowledge distillation. Another category comprises parameter-isolation methods [7], which modify or add network parameters or sub-modules according to task-specific requirements in order to adapt the network architecture during training to new tasks. Replay-based methods [8] store or generate samples or representations from previous data to mitigate catastrophic forgetting. Exemplar-based methods [9], a subset of replay methods, specifically require a rehearsal buffer to store a fixed number of samples from previous classes. In contrast, class-prototype based methods are exemplar-free methods that utilize a network for feature extraction and memorize a set of representative prototypes for each class, which are employed for classification purposes [10]. Recently, pre-trained models (PTMs), such as Vision Transformers (ViT) [11], have demonstrated remarkable progress in generating strong repre-

sentations, rendering them a good choice for CIL scenarios [12]. The generalization capability of PTMs can be combined with parameter-efficient fine-tuning (PEFT) techniques to tackle the different distribution in downstream tasks [13].

In this paper, we propose a class-prototype based incremental learning framework, termed IncSAR, for SAR target recognition. We argue that PTMs can be successfully used in CIL for SAR target recognition reducing time requirements, enabling generalization to new tasks and cross-domain adaptation. IncSAR utilizes a pre-trained ViT and a custom-designed Convolutional Neural Network (CNN), called SAR-CNN, as strong feature extractors, combining them in a late-fusion strategy to take advantage of their complementary strengths. A scale and shift method is employed for the PEFT of the PTM to mitigate the distribution mismatch problem in the downstream dataset. An RPCA module is employed for noise despeckling before CNN feature extraction. The extracted features are randomly projected in a higher-dimensional space to enhance the linear separability, and then they are utilized to extract the class prototypes. A linear discriminant analysis (LDA) [14] approach is used for the decorrelation of prototypes, which are used for classification. The main contributions of the proposed framework are summarized as follows:

- A late-fusion strategy is introduced, combining a pre-trained ViT and a custom-designed CNN as network backbones. A scale and shift method is employed for the PEFT of ViT model.
- IncSAR employs an exemplar-free prototype learning approach, without using a rehearsal buffer. A Linear Discriminant Analysis (LDA) [14] approach is employed to decorrelate the extracted class prototypes.
- Robust Principal Component Analysis (RPCA) [15] is effectively utilized for noise despeckling in SAR imagery further enhancing the classification accuracy of IncSAR.
- Extensive experiments on the MSTAR dataset demonstrate notable gains over state-of-the-art approaches, with average accuracy increasing from 98.05% to 99.63% and performance dropping rate improving from 3.05% to 0.33%. The generalization of IncSAR is also evaluated by combining multiple classes from the OpenSAR-Ship dataset and a series of ablation studies attest to its robustness and effectiveness.

2 Related work

Class incremental learning: CIL methods can be broadly divided into [32]: regularization-based methods (iCaRL [5], LUCIR [6], Foster [9]), parameter-isolation

based methods (DER [7]), replay-based methods (Fetrl [33]), and pre-trained methods [12]. Recent studies focus heavily on pre-trained methods benefiting from the powerful feature extraction capabilities of PTMs, and mainly include prompt-based methods, class-prototype based methods, and model-mixture based methods. Prompt-based methods insert a small number of learnable parameters rather than fully fine-tuning the PTM’s weights (L2P [34], Coda-prompt [35]). Class-prototype based methods extract representative prototypes for each class and utilize them for classification (Adam [36], RanPAC [10], SLCA [37]). These methods can employ a frozen PTM or be combined with PEFT techniques, and they can also utilize prototype decorrelation techniques. The main idea of model-mixture based methods involves ensembling or merging various fine-tuned PTMs into a single model that integrates the representational capabilities of multiple models (PROOF [38], SEED [39], CoFiMA [40]). These methods are highly complementary and can combine different approaches, depending on the priorities of the learning scenario.

Class incremental learning for SAR-ATR: Most existing methods for CIL in SAR-ATR are exemplar-based and rely on a bounded subset of past training data. A weight correction method, named MEDIL, was proposed in [16] that utilizes a hybrid loss function to strike an optimal plasticity-stability trade-off. The CBe-sIL approach [17] introduced a class-boundary selection method using local geometry and statistics, along with a resampling method for data distribution reconstruction. A major issue with replay methods concerns the imbalance between old and new classes due to the limited amount of old class data stored in the rehearsal buffer. Zhou *et al.* [18] proposed a bias-correction layer to tackle the class imbalance problem. The process of selecting exemplars is critical in data replay methods. DCBES [20] utilized a greedy algorithm to select representative exemplar samples based on their density in the feature space. Tang *et al.* [22] proposed a method named HPecIL, that combines replay and weight regularization techniques. HPecIL preserved multiple optimal models from old data, employing a pruning initialization method to remove low-impact nodes of the neural network, and using class-balanced training batches to address the distribution shift in the incremental tasks. Hu *et al.* [23] proposed the addition of extra linear layers after the feature extractor of the network and before each incremental task to generate distilled labels. The ICAC approach [25] was based on anchored class data centers to promote tighter clustering within each class and better separation between classes. ICAC introduced separable learning to mitigate class imbalance, a learning strategy that computes the loss functions for old and new exemplars separately. MLaKDN [26] was proposed as a method that combines classification and feature-level knowledge distillation. Ren *et al.* [27] introduced a dynamic feature embedding network and a hybrid loss function to optimize the proposed method.

Table 1: Summary of SAR-ATR incremental methods

Methods	Regularization	Replay/ Exemplars	Parameter Isolation	Feature Extractor	Dataset	Year
MEDIL [16]	✓	✓		-	MSTAR, OpenSARShip	2023
CBesIL [17]		✓		-	MSTAR	2020
Zhou <i>et al.</i> [18]	✓	✓	✓	ResNet-18 [19]	MSTAR	2022
DCBES [20]		✓		CNN [21]	MSTAR	2023
HPecIL [22]	✓	✓	✓	ResNet-18	MSTAR	2022
Hu <i>et al.</i> [23]	✓	✓		Alexnet [24]	MSTAR	2022
ICAC [25]	✓	✓		CNN	MSTAR, OpenSARShip	2022
MLAKDN [26]	✓	✓		Resnet-18	MSTAR, SAMPLE	2023
DERDN [27]	✓	✓		ODConv [28]	MSTAR, SAMPLE	2024
SSF-IL [29]		✓		ResNet-18	MSTAR	2024
Pan <i>et al.</i> [30]	✓	✓	✓	ViT[11]	MSTAR, CIFAR100	2023
CIL-MMI [31]	✓			ResNet-18	MSTAR	2024

Some recent works utilized PTMs as feature extractors. Gao *et al.* [29] introduced a mechanism for enhancing the linear separability of features, utilizing a Resnet-18. Pan *et al.* [30] proposed employing a ViT combined with a dynamic query navigation module, which was designed to improve the plasticity of the model. An exemplar-free based method, that does not retain any old-class samples was proposed by Li *et al.* [31], employing a mutual information maximization method to avoid the distribution overlap among classes. A comprehensive summary of the discussed SAR-ATR incremental methods is presented in Table 1.

While most studies utilize exemplars, our work introduces an exemplar-free approach based on prototype learning. Furthermore, while previous research has explored the usage of PTMs, we extend the literature by proposing a late-fusion strategy. This leverages the advantages of combining general features extracted from a PTM with specialized features derived by a custom-designed CNN.

3 Methodology

3.1 Background

CIL: Unlike the “traditional” machine learning setting, where a model is trained on all classes with all training data available at once, in CIL a model sequentially receives new training data with additional classes over time. In a more detailed view, in a CIL scenario we assume a sequence of T tasks and their corresponding training sets \mathbf{D}_t for $t \in \{1, 2, \dots, T\}$. A task refers to a set of classes that are disjoint and do not overlap with the classes in other tasks. For each incremental task t , the training set is defined as $\mathbf{D}_t = \{(x_i, y_i)\}_{i=1}^{N_t}$, where N_t is the number of training samples in \mathbf{D}_t , and (x_i, y_i) is a training instance with its corresponding label. Here, $y_i \in Y_t$ and Y_t denotes the label space of task t . We refer to \mathbf{D}_0 as the base task, and all other tasks

as incremental tasks. In typical CIL, it is assumed that there are no overlapping classes between different tasks: $Y_t \cap Y_{t'} = \emptyset$ for $t \neq t'$. During training on task \mathbf{D}_t , only data from this task is accessible; data from previous tasks is not available. We adopt an offline learning setting, where we may process the training data multiple times during the current task before moving to the next. After each task, the trained model is evaluated over all seen classes, represented by the set $\mathcal{Y}_t = \bigcup_{i=1}^t Y_i$. The aim of CIL is to build a classification model that acquires knowledge of all seen classes \mathcal{Y}_t and performs well not only on the ongoing task but also in preserving its performance on previous ones. Particularly, in exemplar-based methods, limited access to old training samples is allowed by storing a small subset of data from previous tasks in a memory buffer, in contrast to exemplar-free methods, which do not retain any previous data.

3.2 IncSAR framework

The proposed framework, called IncSAR, is inspired by RanPAC [10], a class-prototype based method that takes advantage of a PTM’s feature extraction capabilities. The pipeline of IncSAR is demonstrated in Fig. 1. A late-fusion strategy is introduced, comprising two individual branches that take advantage of two different backbones: a pretrained ViT-B/16 model and a custom-designed CNN model. The backbone networks are trained individually during the base task, and then the weights are frozen during incremental tasks. A filtering RPCA module is employed before the CNN model. After the feature extraction, a random projection layer is employed, and the projected features are utilized to compute the class prototypes, while an LDA approach is employed to decorrelate them. Finally, the logits of each branch are integrated to derive the final prediction.

In a more detailed view, our proposed CNN that is inspired by [41], denoted as SAR-CNN, constitutes a simple yet effective model. SAR-CNN is trained from scratch in the base task, and then its weights are frozen

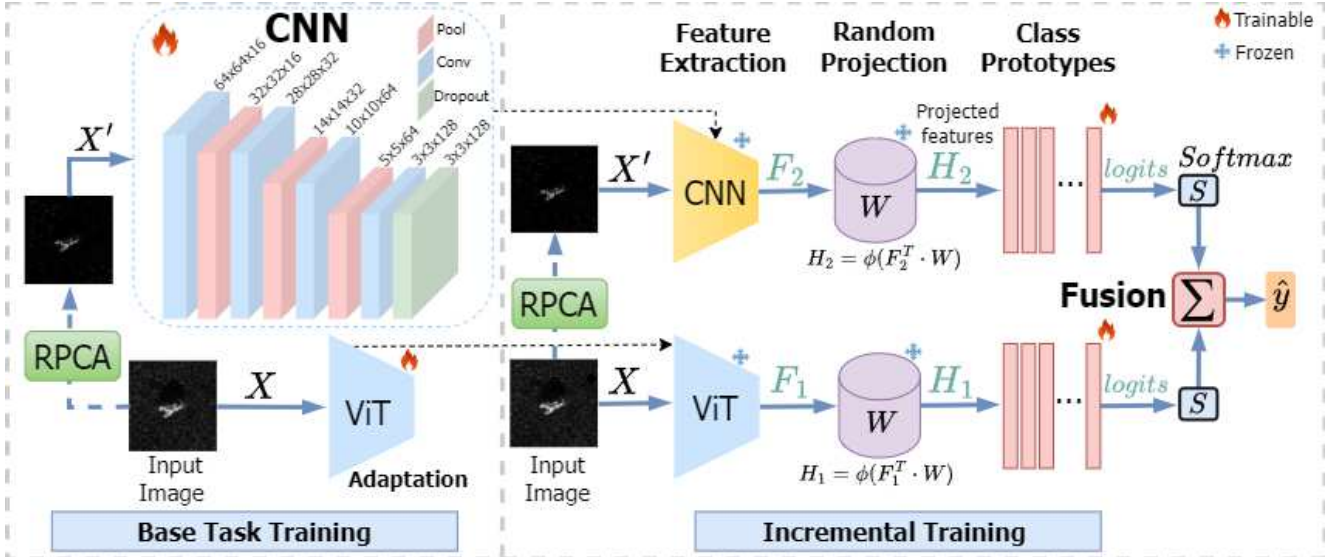


Figure 1: Illustration of IncSAR: A late-fusion approach is employed. The input image feeds a ViT-B/16 network to extract features \mathbf{F}_1 . The input image is passed through the filtering RPCA module, and the filtered output feeds the proposed CNN to extract features \mathbf{F}_2 . The backbone networks are trained only in the base task of CIL, and then their weights are frozen. The extracted features \mathbf{F}_1 , \mathbf{F}_2 are projected into a higher dimensional space using a random projection layer with frozen weights W and an activation function ϕ , giving \mathbf{H}_1 , \mathbf{H}_2 features respectively. During incremental training, the matrices of the decorrelated class prototypes \mathbf{P}_1 , \mathbf{P}_2 are continually updated for each task. The logits \mathbf{L}_1 , \mathbf{L}_2 are passed to a softmax layer S and an element-wise addition layer to derive the final prediction \hat{y} .

during the incremental tasks. The input image \mathbf{X} is filtered by RPCA. The presence of speckle noise in SAR images poses significant challenges, hindering precise analysis and accurate classification. RPCA [15] has been utilized in various applications in computer vision. Here, RPCA is utilized as a pre-processing step to denoise SAR images and improve the classification accuracy of the SAR-CNN. Let \mathbf{X} be a matrix with a dimension of $m \times l$, representing a noisy SAR image. RPCA defines the problem of recovering a low-rank matrix $\mathbf{X}' \in \mathbb{R}^{m \times l}$, which represents the filtered SAR image, from a corrupted data matrix $\mathbf{X} \in \mathbb{R}^{m \times l}$, assuming $\mathbf{X} = \mathbf{X}' + \mathbf{E}$, where $\mathbf{E} \in \mathbb{R}^{m \times l}$ is a sparse error matrix. It is shown that under certain conditions, the matrix \mathbf{X}' can be exactly recovered by the optimization problem:

$$\min_{\mathbf{X}', \mathbf{E}} \|\mathbf{X}'\|_* + \lambda \|\mathbf{E}\|_1 \quad (1)$$

Here $\|\mathbf{X}'\|_*$ represents the nuclear norm of matrix \mathbf{X}' , $\|\mathbf{E}\|_1$ the ℓ_1 -norm of matrix \mathbf{E} and λ is a tuning parameter that balances the two terms. We implement the algorithm proposed by Lin *et al.* [42], which utilizes the techniques of augmented Lagrange multipliers [43] to solve the RPCA problem.

The input layer takes the filtered image \mathbf{X}' , with an input size of 70×70 and is followed by a sequence of 4 convolutional layers, each one followed by a max pooling layer. The activation function for each layer is a ReLU function. The kernel sizes are 7×7 , 5×5 , 3×3 , 3×3 and the numbers of kernels are 16, 32, 64, and 128

respectively. Finally, a dropout layer and a dense layer are applied.

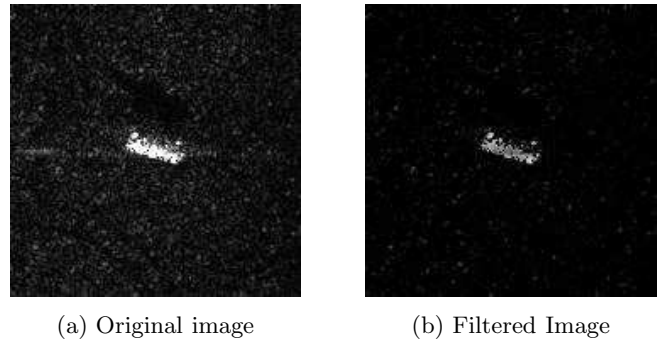


Figure 2: An example of RPCA filtering, employed in MSTAR dataset. On the left, the original SAR image is depicted. On the right, the output of the filtering module is shown.

The pre-trained ViT-B/16 model is fine-tuned exclusively on the base task, and its weights are frozen during the incremental tasks. We employ a scale and shift (SSF) method, which was proposed by Lian *et al.* [44], to adjust the extracted features to match the distribution of the downstream dataset. This method appends an extra SSF layer after each operation layer of the ViT model. Let \mathbf{x}_{in} be the output of an operation layer with a dimension of d . The modulated output \mathbf{x}_o is computed by:

$$\mathbf{x}_o = \gamma \otimes \mathbf{x}_{in} + \delta \quad (2)$$

where \otimes is an element-wise multiplication operator and $\gamma, \delta \in \mathbb{R}^d$ are the scale and shift factors.

During each incremental task, the features \mathbf{F} are extracted individually from each branch. An extra layer, followed by a non-linear function ϕ , is employed after feature extraction to randomly project the features into a higher-dimensional space M . The projected features \mathbf{H} are given by:

$$\mathbf{H} = \phi(\mathbf{F}^\top \mathbf{W}) \quad (3)$$

This feature transformation is employed to enhance linear separability, and its weights \mathbf{W} are frozen and generated randomly only once before the incremental training. Additionally, a variation of linear discriminant analysis (LDA) for continual learning [14] is employed to remove correlations between class prototypes [10]. The Gram Matrix \mathbf{G} of features \mathbf{H} is extracted in an iterative manner:

$$\mathbf{G} = \sum_{t=1}^T \sum_{n=1}^{N_t} \mathbf{H}_{t,n} \otimes \mathbf{H}_{t,n}, \quad (4)$$

The concatenated matrix \mathbf{C} of class prototypes is given by:

$$\mathbf{C} = \sum_{t=1}^T \sum_{n=1}^{N_t} \mathbf{H}_{t,n} \otimes \mathbf{y}_{t,n} \quad (5)$$

where \otimes is the outer product, T is the number of incremental tasks and N_t is the number of training samples in each task. The weights \mathbf{P} represent the decorrelated class prototypes:

$$\mathbf{P} = (\mathbf{G} + \lambda \mathbf{I})^{-1} \mathbf{C} \quad (6)$$

where λ is the ridge regression parameter. Parameter λ is updated after each task and is optimized by randomly dividing the training data for that task using an 80:20 ratio and selecting the value of λ that minimizes the mean square error between targets and the set of predictions. The logits \mathbf{L} are computed by:

$$\mathbf{L} = \mathbf{H}_{\text{test}} \mathbf{P} \quad (7)$$

where \mathbf{H}_{test} refers to the encoded features of a test sample after the random projection layer.

The predictions of each model are integrated to obtain the final decision. A softmax layer S is applied on top of the logits of each model to get the probabilities and an element-wise addition layer to make the final prediction \hat{y} :

$$\hat{y} = \arg \max_{c \in \mathcal{Y}_t} \left(S(\mathbf{L}_1^c) + S(\mathbf{L}_2^c) \right) \quad (8)$$

where $\mathbf{L}_1, \mathbf{L}_2$ are the logits of SAR-CNN and the logits of ViT respectively, calculated for each class c to select the maximum result for the final prediction.

4 Experiments

4.1 Experimental settings

Datasets. To evaluate IncSAR for classifying SAR images, we initially employ the MSTAR dataset [45].

Table 2: Configuration of MSTAR Dataset

Class	Class name	Training set		Testing set	
		Depression	Number	Depression	Number
0	BTR60	17°	256	15°	195
1	T72	17°	232	15°	196
2	2S1	17°	299	15°	274
3	T62	17°	299	15°	273
4	ZIL131	17°	299	15°	274
5	ZSU234	17°	299	15°	274
6	BRDM2	17°	298	15°	274
7	D7	17°	299	15°	274
8	BMP2	17°	233	15°	195
9	BTR70	17°	233	15°	196

MSTAR is a publicly available benchmark dataset of SAR images that contains 10 ground mobile targets, as shown in Table 2. SAR images are acquired at two different angles of depression, i.e., 15° and 17°. Images at 17° are used for training, and images at 15° are used for testing. The OpenSARShip [46] dataset is also employed in the conducted experiments for generalization purposes, as done in [22]. OpenSARShip contains 11,346 SAR ship chips, integrated with automatic identification system (AIS) messages. The dataset covers 17 AIS types collected from 41 Sentinel-1 SAR images. Three ship types are selected, i.e., bulk carrier, container ship, and tanker, under the VV polarization mode. We randomly select 300 samples from each class and split them into training and test sets with an 80:20 ratio. These datasets were selected due to their prevalent use in related literature, as can be seen in Table 1.

Evaluation Protocol. A suite of evaluation metrics is employed to assess the performance of IncSAR. Top-1 accuracy in the t^{th} task is denoted as A_t . The accuracy in the last incremental task, denoted as A_L , is a suitable metric to measure the overall accuracy among all classes. The average incremental accuracy \bar{A} takes into consideration the overall accuracy scores along all incremental tasks: $\bar{A} = \frac{1}{T} \sum_{t=0}^T A_t$. Also, we utilize the performance dropping rate $\text{PD} = A_0 - A_L$ and the performance dropping rate per task $\text{PD}_t = A_0 - A_t$, where A_0 denotes accuracy in the base task and A_t accuracy in the t^{th} incremental task. PD is an established metric in the literature, that tries to quantify how much forgetting takes place in the overall procedure.

Training Details. Experiments are implemented using the PyTorch [47] framework and PILOT [48], a pre-trained model-based continual learning toolbox. Two different data augmentation approaches are employed for each backbone. For ViT-B/16, the original images are simply padded to a size of 224×224 . For SAR-CNN, the training images are filtered by RPCA followed by common transformations, such as cropping to 32×32 , resizing to 70×70 , and random horizontal flipping. The targets in the MSTAR and OpenSARShip datasets are centered in the middle of the image, allowing cropping to discard unwanted noise peripheral to the target. The SAR-CNN branch is trained for 30 epochs and the ViT/B-16 branch for 10 epochs, both us-

ing a learning rate of 0.01, a weight decay of 0.0005, and stochastic gradient descent optimizer with a momentum of 0.9. The dimension of random projection is set to $M = 10000$. To facilitate the replication of our results and ensure the transparency of our research, we provide the source code used in our experiments to the reviewers, as supplementary material.

Table 3: Comparison with prior works across each incremental task on the MSTAR dataset. The base incremental task consists of 4 classes, and each incremental task consists of 1 class.

Method	Accuracy in each task (%)						PD ↓	\bar{A} ↑	
	0	1	2	3	4	5			
iCaRL [5]	70.90	72.85	73.49	76.48	58.95	55.94	52.66	18.24	65.89
adam_adapter [36]	89.13	88.70	87.01	86.65	84.71	80.62	76.99	12.14	84.83
adam_ssf [36]	93.07	94.55	92.40	91.02	90.02	85.64	80.95	12.12	89.66
adam_vpt_deep [36]	80.81	80.86	77.66	79.09	77.97	72.99	70.23	10.58	77.08
MEMO [49]	91.36	93.40	93.61	92.90	91.64	88.83	85.15	6.21	90.98
RanPAC [10]	98.61	<u>98.68</u>	<u>98.12</u>	<u>98.35</u>	<u>97.49</u>	<u>94.93</u>	<u>94.23</u>	4.38	<u>97.20</u>
FOSTER [9]	63.54	84.90	71.27	69.72	67.65	61.01	59.42	<u>4.12</u>	68.21
DualPrompt [50]	85.50	66.17	53.97	45.57	39.43	36.03	33.73	51.77	51.48
CODA-Prompt [35]	27.19	21.04	21.80	16.82	15.63	14.27	13.11	14.08	18.55
Pan et al. [30]	98.49	-	-	-	-	-	74.65	-	-
ICAC [25]	<u>99.49</u>	98.04	96.76	95.65	94.83	93.42	91.76	4.66	96.65
IncSAR (Proposed)	99.89	99.83	99.80	99.15	98.82	98.74	99.38	0.51	99.37

4.2 Competing methods

The proposed IncSAR framework is compared with state-of-the-art incremental learning methods that use PTMs, as well as with state-of-the-art CIL algorithms designed specifically for SAR-ATR recognition. Two main incremental setups consistent with the literature were employed for the evaluation of the proposed framework.

In the first setup, denoted as B4Inc1, the base task comprises 4 classes, while each incremental task consists of a single class. The class order is shown in Table 2, following the same order as in [30]. The results are shown in Table 3. Nine CIL state-of-the-art methods were employed together with two state-of-the-art methods from the field of SAR-ATR, namely, iCaRL, 3 variations of ADAM, MEMO, RanPAC, FOSTER, Dual-Prompt, Coda-Prompt, ICAC, and a method proposed by Pan *et al.* [30]. The PILOT [48] toolbox is used to test the state-of-the-art methods in a standardized manner.

FOSTER, iCaRL, DualPrompt, and CODA-Prompt perform poorly in accurately classifying SAR image vehicles of the MSTAR dataset. The proposed IncSAR achieves an average accuracy of 99.37%, demonstrating very strong performance in classifying SAR images, and outperforming the state-of-the-art RanPAC method, which yields an accuracy of 97.2%. IncSAR also surpasses the state-of-the-art ICAC approach by 7.62% in terms of A_L and by 2.74% in terms of \bar{A} . IncSAR demonstrates a noteworthy percentage improvement of 87.62% regarding PD, attaining 0.51% and outperforming FOSTER, which yields a PD of 4.12%. ICAC is lagging behind IncSAR and FOSTER with a PD of 4.66%.

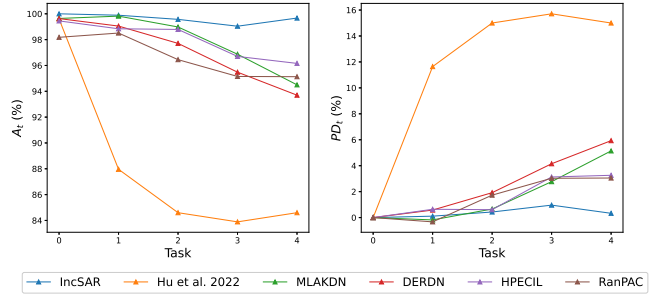


Figure 3: Comparison with state-of-the-art methods on MSTAR dataset. Classification accuracy A_t and performance drop PD_t of each incremental task t are depicted.

Table 4: Comparison with state-of-the-art in each incremental task on the MSTAR dataset. The classes are equally divided into five tasks, with each task consisting of two classes.

Method	Accuracy in each task (%)					PD ↓	\bar{A} ↑
	0	1	2	3	4		
Hu <i>et al.</i> [23]	99.60	87.96	84.60	83.89	84.60	15.00	88.13
SSF-IL [29]	-	-	-	-	-	-	<u>98.05</u>
MLAKDN [26]	<u>99.64</u>	<u>99.82</u>	<u>98.98</u>	<u>96.87</u>	94.50	5.14	97.96
DERDN [27]	99.63	99.05	97.71	95.48	93.70	5.93	97.11
HPecIL [22]	99.45	98.83	98.79	96.70	<u>96.16</u>	3.26	97.92
Zhou <i>et al.</i> [18]	-	-	-	-	-	-	97.73
RanPAC [10]	98.18	98.51	96.45	95.15	95.13	<u>3.05</u>	96.68
IncSAR (Proposed)	100	99.89	99.57	99.04	99.67	0.33	99.63

In the second setup, denoted as B2Inc2, all incremental tasks are equally split, each consisting of two classes. The same class order is employed, as in [22, 27, 26]. Results are shown in Table 4. All methods in the base task demonstrate very accurate results achieving over 99%. As tasks increase sequentially, catastrophic forgetting occurs, leading to performance drops, as shown in Fig. 3. However, IncSAR exhibits robust performance over all incremental tasks, showcasing the lowest PD compared to the state of the art. Experimental results attest to the remarkable ability of IncSAR to resist catastrophic forgetting achieving a PD of 0.33% and outperforming RanPAC, which attains a PD of 3.05%. IncSAR surpasses MLaKDN by 5.62% in A_L and by 4.81% in PD. IncSAR yield an improvement of 3.65% regarding A_L and 89.87% regarding PD, when compared to HPecIL. IncSAR outperforms its competitors resulting in an average accuracy of 99.63%. It should also be noted that IncSAR does not use exemplars, unlike HPecIL, MLaKDN, and DERDN. This makes it an even more challenging scenario, as it lacks direct access to past data, unlike exemplar-based methods, which preserve and replay stored samples to mitigate catastrophic forgetting.

4.3 Evaluation of generalization ability

For the evaluation of the generalization ability of IncSAR, three classes from OpenSarShip are added in the last incremental tasks, as done in [22]. The setup and

Table 5: Results in cross-dataset testing. Three classes of the OpenSarShip dataset are added in the last incremental tasks to evaluate the generalization ability of IncSAR.

Method	Accuracy in each task (%)								PD ↓	\bar{A} ↑
	ZIL131/D7	BTR70/T72	BMP2/BRDM2	T62/BTR60	2S1/ZSU234	Bulk Carrier/Container	Tanker			
	0	1	2	3	4	5	6			
iCaRL [5]	99.27	<u>99.25</u>	93.40	92.32	93.88	90.62	89.99	9.28	94.10	
ECIL [22]	99.45	98.82	98.54	95.31	93.65	94.20	89.34	10.11	95.61	
ECIL+ [22]	<u>99.63</u>	98.51	98.08	96.69	<u>96.41</u>	94.43	92.26	7.37	96.57	
HPecIL [22]	99.45	98.83	<u>98.79</u>	<u>96.70</u>	96.16	<u>95.89</u>	<u>94.07</u>	<u>5.38</u>	<u>97.10</u>	
IncSAR (Proposed)	100	99.89	99.57	99.04	99.67	98.47	96.10	3.90	98.97	

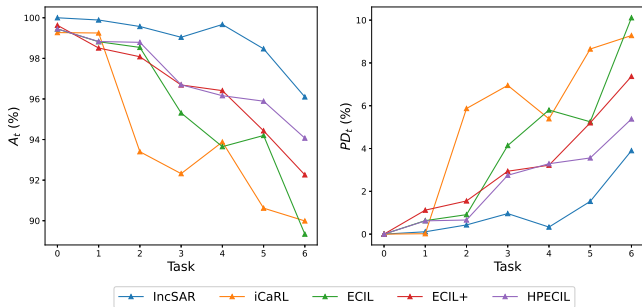


Figure 4: Comparison with state-of-the-art methods for testing the generalization ability of the proposed framework.

experimental results are listed in Table 5. The accuracy in each task and the performance dropping for various state-of-the-art methods are depicted in Fig. 4. Despite the different distribution and varying sizes of targets in the OpenSarShip dataset, IncSAR outperforms its competitors, attaining an average accuracy of 98.97%, while HPecIL is lagging behind deriving an accuracy of 97.1%. IncSAR is also the top performing approach in the last incremental task, demonstrating a noteworthy accuracy of 96.1%, while HPecIL and ECIL+ yielded 94.07% and 92.26%, respectively. The proposed IncSAR demonstrates superior results in all incremental tasks compared to state-of-the-art methods and the iCaRL one, which acts as a baseline. IncSAR derives a value of 3.9 regarding PD, outperforming HPecIL, which attains a value of 5.38. The rest of the methods demonstrate higher values reaching a PD of 10.11 for the ECIL method. Compared to HPecIL, IncSAR improves by 2.15% in A_L and by 27.51% in PD. These results attest to the remarkable efficacy of IncSAR in handling the cross-dataset challenges posed by the OpenSarShip dataset.

4.4 Ablation studies

4.4.1 Contribution analysis of IncSAR modules

The proposed IncSAR framework benefits from multiple modules, including RPCA, SSF adaptation of ViT, and late-fusion of the individual SAR-CNN and ViT branches. To explore the contribution of these modules, a series of experiments were conducted and the results are shown in Table 6. The ablation experiments

were conducted on the MSTAR dataset using the B4Inc1 setup. First, we assess the performance of ViT-B/16 as a network backbone without PEFT, where the models' weights remain frozen throughout the training process. This serves as a baseline to understand the capabilities of the pre-trained ViT-B/16 model without any fine-tuning, achieving 95.34% in terms of A_L . When ViT-B/16 is adapted with the SSF technique, the model improves A_L by 1.98%, showing that if there is sufficient data in the base task, adapting the PTM to the downstream dataset can be effective. We demonstrate the improvement achieved by RPCA filtering, when using the proposed SAR-CNN architecture as a backbone, where IncSAR attains an average accuracy of 98.37% compared to the resulting accuracy without employing the RPCA module. This indicates that RPCA enhances SAR-CNN's ability to provide more distinguishable features, leading to better class separability. Finally, the late-fusion strategy remarkably enhances the detection ability of IncSAR, resulting in an average accuracy of 99.37%. This indicates that combining the specialized features produced by the SAR-CNN with the more general features derived by the pre-trained ViT leads to a significant increase in performance.

Table 6: Ablation studies on multiple components of IncSAR on MSTAR dataset.

Model	SSF	RPCA	Fusion	\bar{A}	A_L
ViT-B/16	x	x	x	98.67	95.34
ViT-B/16	✓	x	x	98.86	97.32
SAR-CNN	x	x	x	96.10	95.26
SAR-CNN	x	✓	x	98.37	98.23
ViT-B/16 + SAR-CNN	✓	✓	✓	99.37	99.38

4.4.2 Comparative analysis of backbone networks

The detection ability of SAR-CNN within the IncSAR framework is evaluated, comparing its performance against a variety of pre-trained backbone networks. Table 7 demonstrates the comparison of the proposed SAR-CNN employing DenseNet-121 [51], ResNet-18 [19], ResNet-101 [19], VGG-19 [52], and CLIP-ViT-L/14 [53] on the MSTAR dataset under the B2Inc2 setup. The experiments utilize the IncSAR framework, as described in Section 3, with the ViT branch remain-

ing consistent, while different networks are tested in the second branch of IncSAR. It is observed that freezing the weights demonstrated better performance compared to fine-tuning them during the base task. SAR-CNN is a lightweight network, that shows remarkable memory efficiency with only 140k parameters, outperforming the rest of the backbones that require much higher memory budgets. When compared to ResNet-101, SAR-CNN leads to a performance improvement by 5.17% in terms of average accuracy and by 4.91% in terms of performance drop. SAR-CNN demonstrates a performance improvement of 4.81% regarding average accuracy compared to CLIP-ViT-L/14, most likely due to the significant gap in the MSTAR’s data distribution. DenseNet-121 achieves the second-best performance yielding 98.24% in terms of \bar{A} and 2.35% in terms of PD, while comprises 7M parameters. VGG-19 is lagging behind SAR-CNN and DenseNet-121, yielding an \bar{A} of 98.03% and a PD of 3.46%.

Table 7: Comparative analysis of different backbone networks in IncSAR framework.

Network	Params	\bar{A}	PD	A_L
DenseNet-121 [51]	7M	<u>98.24</u>	<u>2.35</u>	<u>97.65</u>
ResNet-18 [19]	11M	92.67	10.06	89.94
ResNet-101 [19]	44M	94.46	5.24	94.76
VGG-19 [52]	140M	98.03	3.46	96.54
CLIP-ViT-L/14 [53]	303M	94.82	7.67	92.33
SAR-CNN	140K	99.63	0.33	99.67

4.4.3 IncSAR evaluation on limited data scenarios

Subsets of the MSTAR dataset are randomly selected to assess the detection ability of the proposed framework under various reduced training data scenarios. Specifically, three different scenarios are tested, employing 80%, 50%, and 20% of the initial training data. When 50% of the initial training data are employed, IncSAR yields an average accuracy of 98.64%, outperforming state-of-the-art MLaKDN and HPECIL methods, which attain 97.96% and 97.92%, respectively. In the challenging scenario of retaining only 20% of samples, IncSAR demonstrates a noteworthy performance of 96.24% in terms of average accuracy, which is slightly lower than MLaKDN by 1.72%. These results underscore IncSAR’s efficiency in detecting SAR images with limited training data, highlighting its capability to generalize well in real-world scenarios. Experimental results are shown in Table 8.

5 Conclusion

A novel incremental learning framework for SAR target recognition has been proposed based on exemplar-free prototype learning. RPCA is utilized to filter the

Table 8: Ablation study of the IncSAR framework under training in different portions of the MSTAR dataset.

Method	Size (%)	Accuracy in each task (%)					PD ↓	\bar{A} ↑
		0	1	2	3	4		
IncSAR	100	100	99.89	99.57	99.04	99.67	0.33	99.63
	80	100	99.89	97.87	<u>97.55</u>	97.40	2.60	98.52
	50	100	99.89	98.58	97.18	<u>97.57</u>	<u>2.43</u>	<u>98.64</u>
	20	99.82	99.47	95.74	92.38	93.81	6.01	96.24
MLaKDN [26]	100	99.64	99.82	<u>98.98</u>	96.87	94.50	5.14	97.96
HPECIL [22]	100	99.45	98.83	98.79	96.70	96.16	3.26	97.92

speckle noise of SAR images, and a random projection layer is used for better linear separability of features. A late-fusion strategy is employed, utilizing a ViT network backbone to extract more generalized features and the designed SAR-CNN for more specialized features. IncSAR achieves a noteworthy balance between stability and plasticity and demonstrates remarkable performance on the MSTAR and OpenSarShip datasets, outperforming state-of-the-art approaches. A series of experiments have also been conducted to evaluate the performance of the proposed modules and attest to the robustness and the generalization ability of the proposed framework.

Acknowledgments

This project has received funding from the FaRADAI project (ref. 101103386) funded by the European Commission under the European Defence Fund. Views and opinions expressed are however those of the author(s) only and do not necessarily reflect those of the European Union or the European Commission. Neither the European Union nor the granting authority can be held responsible for them.

References

- [1] A. Passah, S.N. Sur, B. Paul, and D. Kandar. Sar image classification: A comprehensive study and analysis. *IEEE Access*, 10:20385–20399, 2022. 1
- [2] J. Li, Z. Yu, L. Yu, P. Cheng, J. Chen, and C. Chi. A comprehensive survey on sar atr in deep-learning era. *Remote Sens.*, 15(5):1454, 2023. 1
- [3] M. McCloskey and N. J. Cohen. Catastrophic interference in connectionist networks: The sequential learning problem. In *Psychology of learning and motivation*, volume 24, pages 109–165. Elsevier, 1989. 1
- [4] G. Wu, S. Gong, and P. Li. Striking a balance between stability and plasticity for class-incremental learning. In *IEEE/CVF Int. Conf. Comput. Vis.*, pages 1124–1133, 2021. 1
- [5] S. Rebuffi, A. Kolesnikov, G. Sperl, and C. Lampert. ical: Incremental classifier and representation learning. In *IEEE Conf. Comput. Vis. Pattern Recog. Worksh.*, pages 2001–2010, 2017. 1, 2, 6, 7
- [6] S. Hou, X. Pan, C. C. Loy, Z. Wang, and D. Lin. Learning a unified classifier incrementally via rebalancing. In

- IEEE/CVF Int. Conf. Comput. Vis.*, pages 831–839, 2019. **1, 2**
- [7] P. Buzzega, M. Boschini, A. Porrello, D. Abati, and S. Calderara. Dark experience for general continual learning: a strong, simple baseline. *Adv. Neural Inf. Process. Syst.*, 33:15920–15930, 2020. **1, 2**
- [8] L. Wang, X. Zhang, H. Su, and J. Zhu. A comprehensive survey of continual learning: Theory, method and application. *IEEE Trans. Pattern Anal. Mach. Intell.*, 2024. **1**
- [9] F.-Y. Wang, D.-W. Zhou, H.-J. Ye, and D.-C. Zhan. Foster: Feature boosting and compression for class-incremental learning. In *Eur. Conf. Comput. Vis.*, pages 398–414. Springer, 2022. **1, 2, 6**
- [10] M. McDonnell, D. Gong, A. Parvaneh, E. Abbasnejad, and A. van den Hengel. Ranpac: Random projections and pre-trained models for continual learning. *Adv. Neural Inf. Process. Syst.*, 36, 2024. **1, 2, 3, 5, 6**
- [11] A. Dosovitskiy, L. Beyer, A. Kolesnikov, D. Weissenborn, X. Zhai, T. Unterthiner, M. Dehghani, M. Minderer, G. Heigold, S. Gelly, et al. An image is worth 16x16 words: Transformers for image recognition at scale. *arXiv preprint arXiv:2010.11929*, 2020. **1, 3**
- [12] D.-W. Zhou, H.-L. Sun, J. Ning, H.-J. Ye, and D.-C. Zhan. Continual learning with pre-trained models: A survey. *arXiv preprint arXiv:2401.16386*, 2024. **2**
- [13] G. Burghouts, K. Schutte, M. Kruihof, W. Huizinga, F. Ruis, and H. Kuijff. Synthesizing classifiers from prior knowledge. *Proceedings Copyright*, pages 47–58, 2024. **2**
- [14] A. Panos, Y. Kobe, D. O. Reino, R. Aljundi, and R. E. Turner. First session adaptation: A strong replay-free baseline for class-incremental learning. In *IEEE/CVF Int. Conf. Comput. Vis.*, pages 18820–18830, 2023. **2, 5**
- [15] J. Wright, Y. Peng, Y. Ma, A. Ganesh, and S. Rao. Robust principal component analysis: exact recovery of corrupted low-rank matrices by convex optimization. In *22nd Int. Conf. Neural Inf. Process. Systems*, page 2080–2088, 2009. **2, 4**
- [16] H. Huang, F. Gao, J. Wang, A. Hussain, and H. Zhou. An incremental sar target recognition framework via memory-augmented weight alignment and enhancement discrimination. *IEEE Trans. Geosci. and Remote Sens.*, 2023. **2, 3**
- [17] S. Dang, Z. Cao, Z. Cui, Y. Pi, and N. Liu. Class boundary exemplar selection based incremental learning for automatic target recognition. *IEEE Trans. Geosci. and Remote Sens.*, 58(8):5782–5792, 2020. **2, 3**
- [18] Y. Zhou, S. Zhang, X. Sun, F. Ma, and F. Zhang. Sar target incremental recognition based on hybrid loss function and class-bias correction. *Applied Sciences*, 12(3):1279, 2022. **2, 3, 6**
- [19] K. He, X. Zhang, S. Ren, and J. Sun. Deep residual learning for image recognition. In *IEEE Conf. Comput. Vis. Pattern Recog.*, pages 770–778, 2016. **3, 7, 8**
- [20] B. Li, Z. Cui, Y. Sun, J. Yang, and Z. Cao. Density coverage-based exemplar selection for incremental sar automatic target recognition. *IEEE Trans. Geosci. and Remote Sens.*, 2023. **2, 3**
- [21] J. Liu, X. Fu, K. Liu, M. Wang, C. Zhang, and Q. Su. Spotlight sar image recognition based on dual-channel feature map convolutional neural network. In *2019 IEEE 4th Int. Conf. Signal and Image Process.*, pages 65–69. IEEE, 2019. **3**
- [22] J. Tang, D. Xiang, F. Zhang, F. Ma, Y. Zhou, and H. Li. Incremental sar automatic target recognition with error correction and high plasticity. *IEEE J. Selected Topics in Applied Earth Observations and Remote Sens.*, 15:1327–1339, 2022. **2, 3, 5, 6, 7, 8**
- [23] C. Hu, M. Hao, W. Wang, Y. Yang, and D. Wu. Incremental learning using feature labels for synthetic aperture radar automatic target recognition. *IET Radar, Sonar & Navigation*, 16(11):1872–1880, 2022. **2, 3, 6**
- [24] A. Krizhevsky, I. Sutskever, and G. E Hinton. Imagenet classification with deep convolutional neural networks. *Adv. Neural Inf. Process. Syst.*, 25, 2012. **3**
- [25] B. Li, Z. Cui, Z. Cao, and J. Yang. Incremental learning based on anchored class centers for sar automatic target recognition. *IEEE Trans. Geosci. and Remote Sens.*, 60:1–13, 2022. **2, 3, 6**
- [26] X. Yu, F. Dong, H. Ren, C. Zhang, L. Zou, and Y. Zhou. Multilevel adaptive knowledge distillation network for incremental sar target recognition. *IEEE Trans. Geosci. and Remote Sens.*, 20:1–5, 2023. **2, 3, 6, 8**
- [27] H. Ren, F. Dong, R. Zhou, X. Yu, L. Zou, and Y. Zhou. Dynamic embedding relation distillation network for incremental sar automatic target recognition. *IEEE Trans. Geosci. and Remote Sens.*, 2024. **2, 3, 6**
- [28] C. Li, A. Zhou, and A. Yao. Omni-dimensional dynamic convolution. *arXiv preprint arXiv:2209.07947*, 2022. **3**
- [29] F. Gao, L. Kong, R. Lang, J. Sun, J. Wang, A. Hussain, and H. Zhou. Sar target incremental recognition based on features with strong separability. *IEEE Trans. Geosci. and Remote Sens.*, 2024. **3, 6**
- [30] Q. Pan, K. Liao, X. He, Z. Bu, and J. Huang. A class-incremental learning method for sar images based on self-sustainment guidance representation. *Remote Sens.*, 15(10):2631, 2023. **3, 6**
- [31] B. Li, Z. Cui, H. Wang, Y. Deng, J. Ma, J. Yang, and Z. Cao. Sar incremental automatic target recognition based on mutual information maximization. *IEEE Trans. Geosci. and Remote Sens.*, 2024. **3**
- [32] S. Qiang, X. Lin, Y. Liang, J. Wan, and D. Zhang. Fett: Continual class incremental learning via feature transformation tuning. *arXiv preprint arXiv:2405.11822*, 2024. **2**
- [33] G. Petit, A. Popescu, H. Schindler, D. Picard, and B. Delezoide. Fetril: Feature translation for exemplar-free class-incremental learning. In *IEEE/CVF Winter Conf. Appl. Comput. Vis.*, pages 3911–3920, 2023. **2**
- [34] Z. Wang, Z. Zhang, C.-Y. Lee, H. Zhang, R. Sun, X. Ren, G. Su, V. Perot, J. Dy, and T. Pfister. Learning to prompt for continual learning. In *IEEE/CVF Int. Conf. Comput. Vis.*, pages 139–149, 2022. **2**
- [35] J. S. Smith, L. Karlinsky, V. Gutta, P. Cascante-Bonilla, D. Kim, A. Arbelle, R. Panda, R. Feris, and Z. Kira. Coda-prompt: Continual decomposed attention-based prompting for rehearsal-free continual learning. In

- PIEEE/CVF Int. Conf. Comput. Vis.*, pages 11909–11919, 2023. 2, 6
- [36] D.-W. Zhou, H.-J. Ye, D.-C. Zhan, and Z. Liu. Revisiting class-incremental learning with pre-trained models: Generalizability and adaptivity are all you need. *arXiv preprint arXiv:2303.07338*, 2023. 2, 6
- [37] G. Zhang, L. Wang, G. Kang, L. Chen, and Y. Wei. Sica: Slow learner with classifier alignment for continual learning on a pre-trained model. In *IEEE/CVF Int. Conf. Comput. Vis.*, pages 19148–19158, 2023. 2
- [38] D.-W. Zhou, Y. Zhang, J. Ning, H.-J. Ye, D.-C. Zhan, and Z. Liu. Learning without forgetting for vision-language models. *arXiv preprint arXiv:2305.19270*, 2023. 2
- [39] G. Rypeść, S. Cygert, V. Khan, T. Trzciński, B. Zieliński, and B. Twardowski. Divide and not forget: Ensemble of selectively trained experts in continual learning. *arXiv preprint arXiv:2401.10191*, 2024. 2
- [40] I. E. Marouf, S. Roy, E. Tartaglione, and S. Lathuilière. Weighted ensemble models are strong continual learners. *arXiv preprint arXiv:2312.08977*, 2023. 2
- [41] R. Shang, J. Wang, L. Jiao, R. Stolkin, B. Hou, and Y. Li. Sar targets classification based on deep memory convolution neural networks and transfer parameters. *IEEE J. Selected Topics in Applied Earth Observations and Remote Sens.*, 11(8):2834–2846, 2018. 3
- [42] Z. Lin, Minming Chen, and Y. Ma. The augmented lagrange multiplier method for exact recovery of corrupted low-rank matrices. *J. Structural Biology*, 181 2:116–27, 2010. 4
- [43] D. P. Bertsekas. *Constrained Optimization and Lagrange Multiplier Methods*. Academic press, 1982. 4
- [44] D. Lian, D. Zhou, J. Feng, and X. Wang. Scaling & shifting your features: A new baseline for efficient model tuning. *Adv. Neural Inf. Process. Syst.*, 35:109–123, 2022. 4
- [45] T. D. Ross, S. W. Worrell, V. J. Velten, J. C. Mossing, and M. L. Bryant. Standard sar atr evaluation experiments using the mstar public release data set. In *Algorithms for Synthetic Aperture Radar Imagery V*, volume 3370, pages 566–573. SPIE, 1998. 5
- [46] L. Huang, B. Liu, B. Li, W. Guo, W. Yu, Z. Zhang, and W. Yu. Opensarship: A dataset dedicated to sentinel-1 ship interpretation. *IEEE J. Selected Topics in Applied Earth Observations and Remote Sens.*, 11(1):195–208, 2017. 5
- [47] A. Paszke, S. Gross, F. Massa, A. Lerer, J. Bradbury, G. Chanan, T. Killeen, Z. Lin, N. Gimelshein, L. Antiga, et al. Pytorch: An imperative style, high-performance deep learning library. *Adv. Neural Inf. Process. Syst.*, 32, 2019. 5
- [48] H.-L. Sun, D.-W. Zhou, H.-J. Ye, and D.-C. Zhan. Pilot: A pre-trained model-based continual learning toolbox. *arXiv preprint arXiv:2309.07117*, 2023. 5, 6
- [49] D. Zhou, Q. Wang, H. Ye, and D. Zhan. A model or 603 exemplars: Towards memory-efficient class-incremental learning. *arXiv preprint arXiv:2205.13218*, 2022. 6
- [50] Y. Yang, W. Lei, P. Huang, J. Cao, J. Li, and T. Chua. A dual prompt learning framework for few-shot dialogue state tracking. In *ACM Web Conf. 2023*, pages 1468–1477, 2023. 6
- [51] G. Huang, Z. Liu, L. Van Der Maaten, and K. Q Weinberger. Densely connected convolutional networks. In *IEEE Conf. Comput. Vis. Pattern Recog.*, pages 4700–4708, 2017. 7, 8
- [52] K. Simonyan and A. Zisserman. Very deep convolutional networks for large-scale image recognition. *arXiv preprint arXiv:1409.1556*, 2014. 7, 8
- [53] A. Radford, J. W. Kim, C. Hallacy, A. Ramesh, G. Goh, S. Agarwal, G. Sastry, A. Askell, P. Mishkin, J. Clark, et al. Learning transferable visual models from natural language supervision. In *Int. Conf. Machine Learning*, pages 8748–8763, 2021. 7, 8